IEEE Access
Multidisciplinary ⋮ Rapid Review ⋮ Open Access Journal

Received 30 August 2024, accepted 16 September 2024, date of publication 18 September 2024,
date of current version 30 September 2024.

Digital Object Identifier 10.1109/ACCESS.2024.3463424

RESEARCH ARTICLE

New Approach to Improve Starting Performance of Induction Motor Based on Optimal Starting Frequency

HAIXU CHEN[1], CHAO BI[2], (Senior Member, IEEE), SEN LI[3], ZHEN PENG[4], AND ZHONGXIAN CHEN[1]

[1]College of Energy Engineering, Huanghuai University, Zhumadian, Henan 463000, China
[2]Fortior Technology (Shenzhen) Company Ltd., Shenzhen 518000, China
[3]School of Electrical and Information Engineering, Zhengzhou University, Zhengzhou 450001, China
[4]School of Automotive and Traffic Engineering, Hubei University of Arts and Science, Xiangyang, Hubei 441053, China

Corresponding author: Haixu Chen (chenhaixu@huanghuai.edu.cn)

This work was supported in part by the Scientific and Technological Research Project in Henan Province under Grant 242102321090, and in part by the Program for Innovative Research Team (in Science and Technology) in University of Henan Province under Grant 24IRTSTHN020.

ABSTRACT The starting performance of induction motor (IM) has a prominent influence on the redundancy design and cost control of motor drivers. To make the starting torque as high as possible under the special setting of starting current, a new approach for improving the starting performance of three-phase IM is proposed in this paper. First, the frequency characteristic of the starting torque, which is different from the optimal starting torque per ampere (OSTPA) proposed by the author previously, is investigated based on the universal T-type equivalent model that considers the iron loss. The analysis results confirm the existence of an optimal starting frequency (OSF), which makes the starting torque much higher than that at rated frequency. Secondly, complete discussions of starting initial values are reported and discussed, including starting voltage and motor parameters. Then, the step-by-step starting algorithms based on OSF are provided. Finally, the OSF and its starting strategy are tested on a rapid control prototype system, and the comparison between computed and measured results confirms the feasibility and effectiveness of the proposed approach.

INDEX TERMS Induction motor, T-type equivalent circuit, starting performance, optimal starting frequency, maximum starting torque.

I. INTRODUCTION

Excessive starting current will result in overheating and higher energy consumption of the induction motor (IM) [1], [2], and the current redundancy has to be considered and discussed, which directly increases the cost of motor drivers in industrial applications.

The conventional method of reduced-voltage starting weakens the starting current, however weakens the starting torque as well, which basically hard to solve the motor starting problem [3], [4], [5], [6]. For solving the problems of large inrush current and insufficient starting torque of IM, in addition to optimizing the electromagnetic structure design to improve starting torque [7], [8], [9], [10], [11], [12], [13], many researchers try to solve this problem by driving control. Badr and Alolah [14] and Hu et al. [15] proposed to establish an excitation field for single-phase pre-starting, and then switch to AC operation to achieve the starting process. Nagata et al. proposed a vector control method to adjust the slip angle frequency for IM starting [16].

Soft starter is also a common method to solve the starting problem of IMs, Nafeesa and George believed that the optimal trigger angle of thyristor is closely related to the motor parameters, and can be used to reduce the starting time [17]. Nied et al. used the stator flux estimation method to control the soft starter's electromagnetic torque [18]. In [19], the multifunctional series compensator is used to realize flexible regulation of the motor terminal voltage, and to ensure

The associate editor coordinating the review of this manuscript and approving it for publication was R. K. Saket.

that the motor inrush current and harmonic disturbances are small by injecting changing virtual impedance based on the dynamic voltage-division principle. In [20], [21], [22], [23], [24], and [25], the discrete frequency control was investigated to achieve the purpose of small inrush current and large starting torque in motors, but these discrete frequencies have nothing to do with the starting mechanism of the motor, and also nothing to do with its electromagnetic torque [22], [23], [24], [25], [26].

In a previous study [26], the authors proposed the existence of optimal starting frequency (OSF) by investigating the IM to produce the optimal starting torque per ampere (OSTPA). This paper can be considered a natural and necessary continuation of that one, investigating the action mechanism between starting torque and OSF from a different perspective. On this basis, an effective starting algorithm is proposed to realize IM starting at maximum starting torque within the safe current range of motor driver, optimizing the starting performance and reducing the current redundancy for the motor driver.

It is important to highlight that this paper deals with a three-phase induction motor with symmetrical windings. As the theoretical analysis is developed in a general way, it can be applied to the starting process of both single-phase and three-phase motors, both wound-rotor and squirrel-cage rotor.

II. ANALYSIS OF TORQUE-FREQUENCY CHARACTERISTIC

As is well known, three-phase IM with symmetric windings can be easily computed by using the single-phase equivalent circuit. T-type equivalent model considering the iron loss of IM is adopted here for analysis, and all parameters of the rotor branch have been referred to the stator side.

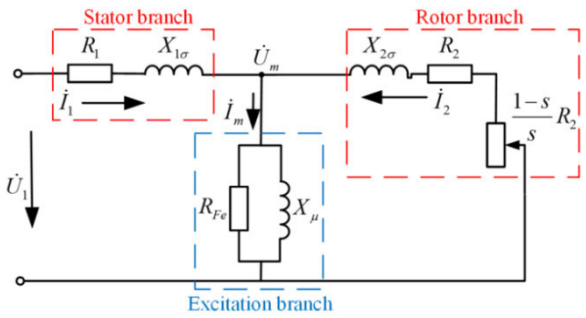

FIGURE 1. T-type equivalent circuit of induction motor.

For the circuit topology shown in Fig. 1, the expression of the excitation voltage can be obtained as

$$\begin{aligned}\dot{U}_{\mathrm{m}} &= \frac{U_1}{\left(1/jX_\mu + 1/R_{\mathrm{Fe}} + 1/Z_2 + 1/Z_1\right)Z_1} \\ &= \frac{jR_{\mathrm{Fe}}X_\mu Z_2 U_1}{R_{\mathrm{Fe}}Z_1Z_2 + jX_\mu\left(Z_1R_{\mathrm{Fe}} + Z_2R_{\mathrm{Fe}} + Z_1Z_2\right)}\end{aligned} \tag{1}$$

where U_1 is the input voltage of IM, U_{m} is the excitation voltage, R_{Fe} is the iron loss resistance, X_μ is the magnetizing reactance, Z_1 is the stator impedance, and Z_2 is the rotor impedance. Z_1 and Z_2 can be expressed as

$$Z_1 = R_1 + jX_{1\sigma} \tag{2}$$

$$Z_2 = R_3 + jX_{2\sigma} \tag{3}$$

$$R_3 = R_2/s \tag{4}$$

where R_1 and $X_{1\sigma}$ are the stator resistance and leakage reactance, respectively. R_2 and $X_{2\sigma}$ are the rotor resistance and leakage reactance referred to stator side, respectively. s is the slip of IM.

By using (5)–(6), the stator current and rotor current of the model can be represented, respectively

$$\begin{aligned}\dot{I}_1 &= \frac{U_1 - \dot{U}_{\mathrm{m}}}{Z_1} \\ &= \frac{R_3R_{\mathrm{Fe}} - X_{2\sigma}X_\mu + j(R_{\mathrm{Fe}}X_{2\sigma} + R_3X_\mu + R_{\mathrm{Fe}}X_\mu)}{C_{Re} + jC_{Im}}U_1\end{aligned} \tag{5}$$

$$\dot{I}_2 = \frac{\dot{U}_{\mathrm{m}}}{Z_2} = \frac{jR_{\mathrm{Fe}}X_\mu}{C_{Re} + jC_{Im}}U_1 \tag{6}$$

where the coefficient of the denominator term

$$\begin{aligned}C_{Re} = {} & R_{\mathrm{Fe}}\left(R_1R_3 - X_{1\sigma}X_{2\sigma} - X_{1\sigma}X_\mu - X_{2\sigma}X_\mu\right) \\ & - \left(R_3X_{1\sigma} + R_1X_{2\sigma}\right)X_\mu\end{aligned} \tag{7}$$

$$\begin{aligned}C_{Im} = {} & R_{\mathrm{Fe}}\left(R_3X_{1\sigma} + R_1X_{2\sigma} + R_1X_\mu + R_3X_\mu\right) \\ & + X_\mu\left(R_1R_3 - X_{1\sigma}X_{2\sigma}\right)\end{aligned} \tag{8}$$

According to the power relation of IM, the electromagnetic torque can be obtained as

$$T_{\mathrm{e}} = \frac{3I_2^2R_2}{s\Omega_{\mathrm{s}}} = \frac{3pR_2(R_{\mathrm{Fe}}X_\mu U_1)^2}{\omega s\left(C_{Re}^2 + C_{Im}^2\right)} \tag{9}$$

where T_{e} is the electromagnetic torque, Ω_s is the synchronous angular velocity, p is the pole pair number, and the voltage angular frequency $\omega = p\Omega_s$.

Substituting (4) into (9), the torque-slip characteristics of IM can be expressed as

$$T_e = \frac{3spR_2(R_{\mathrm{Fe}}X_\mu U_1)^2}{\omega(A_1 + A_2s + A_3s^2)} \tag{10}$$

where the coefficient

$$\begin{cases} A_1 = R_2^2\left\{R_{Fe}^2\left(R_1^2 + X_{1\sigma}^2\right) + 2R_{Fe}^2X_{1\sigma}X_\mu \right. \\ \qquad \left. + \left[(R_1 + R_{Fe})^2 + X_{1\sigma}^2\right]X_\mu^2\right\} \\ A_2 = 2R_2R_{Fe}\left[R_1\left(R_1 + R_{Fe}\right) + X_{1\sigma}^2\right]X_\mu^2 \\ A_3 = R_{Fe}^2\left[X_{1\sigma}X_{2\sigma} + \left(X_{1\sigma} + X_{2\sigma}\right)X_\mu\right]^2 \\ \qquad + R_1^2\left[X_{2\sigma}^2X_\mu^2 + R_{Fe}^2\left(X_{2\sigma} + X_\mu\right)^2\right] \\ \qquad + \left(2R_1R_{Fe} + X_{1\sigma}^2\right)X_{2\sigma}^2X_\mu^2 \end{cases} \tag{11}$$

Let

$$\frac{\delta T_{\mathrm{e}}}{\delta s} = 0 \tag{12}$$

Equation (13) then can be obtained

$$pR_2\left(A_3s^2 - A_1\right)U_1^2R_{\mathrm{Fe}}^2X_\mu^2 = 0 \tag{13}$$

According to the mechanical characteristic of IM, the solution of (13) is the slip, at which the maximum electromagnetic torque T_{emax} can be achieved, i.e., the critical slip rate s_{m}.

$$s_{\mathrm{m}} = \sqrt{A_1/A_3} \tag{14}$$

$$T_{\mathrm{e\,max}} = \frac{3pR_2(R_{\mathrm{Fe}}X_\mu U_1)^2}{\omega(2\sqrt{A_1A_3}+A_2)} \tag{15}$$

From (14)-(15) it can be seen that s_{m} is independent of the motor terminal voltage U_1, and is only influenced by the motor parameters, in particular by R_2. T_{emax} is proportional to the square of U_1, and is theoretically the maximum limit at which the starting torque can be reached.

The frequency characteristics of maximum torque of IM are analyzed in detail below. Constructing the function

$$P(\omega) = s_{\mathrm{m}}^2 A_3 - A_1 \tag{16}$$

The maximum torque can thus be expressed as the zeros of function (16). Taking into account the complexity of IM system under the variable frequency drive, the parameters changes influenced by temperature, magnetic saturation and skin effect are ignored here for a while. The changes of the magnetizing reactance, the stator and rotor leakage reactance with frequency must be considered

$$\begin{cases} X_{1\sigma} = \omega L_{1\sigma} \\ X_{\mu} = \omega L_{\mu} \\ X_{2\sigma} = \omega L_{2\sigma} \end{cases} \tag{17}$$

where $L_{1\sigma}$ is the stator leakage inductance, $L_{2\sigma}$ is the rotor leakage inductance, L_μ is the magnetizing inductance.

Substituting coefficient (11) and expression (17) into (16), then $P(\omega)$ can be obtained as

$$P(\omega) = B_1\omega^6 + B_2\omega^4 + B_3\omega^2 + B_4 \tag{18}$$

where the coefficient

$$\begin{cases} B_1 = s_m^2 L_{1\sigma}^2 L_{2\sigma}^2 L_\mu^2 \\ B_2 = s_m^2\left[L_{2\sigma}L_\mu + L_{1\sigma}\left(L_{2\sigma}+L_\mu\right)\right]^2 R_{Fe}^2 \\ \quad +L_\mu^2\left(s_m^2 L_{2\sigma}^2 R_1^2 + 2s_m^2 L_{2\sigma}^2 R_1 R_{Fe} - R_2^2 L_{1\sigma}^2\right) \\ B_3 = \left[s_m^2\left(L_{2\sigma}+L_\mu\right)^2 R_1^2 - R_2^2\left(L_{1\sigma}+L_\mu\right)^2\right] R_{Fe}^2 \\ \quad -(R_1^2 + 2R_1R_{Fe})R_2^2 L_\mu^2 \\ B_4 = -R_2^2 R_1^2 R_{Fe}^2 \end{cases} \tag{19}$$

Since the coefficient B_1 is the square product of three small values of inductor, and can be neglected whether the iron loss resistance is considered or not, thus $P(\omega)$ can be simplified as

$$P(\omega) = B_2\omega^4 + B_3\omega^2 + B_4 \tag{20}$$

The zeros of function (20) is just the voltage angular frequency at maximum torque of three-phase IM, and can be expressed as

$$\omega_{\mathrm{m}} = \sqrt{\frac{\sqrt{B_3^2 - 4B_2B_4} - B_3}{2B_2}} \tag{21}$$

Then the drive power supply frequency is

$$f_m = \frac{1}{2\pi}\sqrt{\frac{\sqrt{B_3^2 - 4B_2B_4} - B_3}{2B_2}} \tag{22}$$

the maximum torque of IM can be obtained as

$$T_{\mathrm{e\,max}} = \frac{3pR_2(R_{\mathrm{Fe}}X_\mu U_1)^2}{\omega_m(2\sqrt{A_1(\omega_m)A_3(\omega_m)}+A_2(\omega_m))} \tag{23}$$

where the coefficient A_1, A_2, A_3 are all frequency response functions

$$\begin{cases} A_1(\omega) = R_2^2 L_{1\sigma}^2 L_\mu^2 \omega^4 + R_2^2\left[L_{1\sigma}^2 R_{Fe}^2 + 2L_{1\sigma}L_\mu R_{Fe}^2 \right. \\ \quad \left. +L_\mu^2(R_1+R_{Fe})^2\right]\omega^2 + R_2^2 R_1^2 R_{Fe}^2 \\ A_2(\omega) = 2R_2 L_{1\sigma}^2 L_\mu^2 R_{Fe}\omega^4 + 2R_2 L_\mu^2 R_1 R_{Fe}(R_1+R_{Fe})\omega^2 \\ A_3(\omega) = \omega^6 L_{1\sigma}^2 L_{2\sigma}^2 L_\mu^2 + \omega^4\left\{L_{2\sigma}^2 L_\mu^2(R_1^2 + 2R_1R_{Fe}) \right. \\ \quad \left. + \left[L_{2\sigma}L_\mu + L_{1\sigma}\left(L_{2\sigma}+L_\mu\right)\right]^2 R_{Fe}^2\right\} \\ \quad +\omega^2\left(L_{2\sigma}+L_\mu\right)^2 R_1^2 R_{Fe}^2 \end{cases} \tag{24}$$

In particular, when $s_{\mathrm{m}} = 1$, the motor starting torque is equal to the maximum torque T_{emax}, then the motor starting frequency f_{st} is

$$f_{\mathrm{st}} = f_m|_{s_m=1} \tag{25}$$

Equation (25) can be used to calculate the OSF, i.e., the IM drive frequency at which the maximum starting torque (MST) can be obtained. Similarly, in the non-stationary state of IM, by using equivalent parameters and critical slip s_{m}, the drive frequency under the maximum operation torque can also be obtained from (22).

III. DETERMINATIONS OF IM STARTING PARAMETERS

A. DETERMINATIONS OF IM EQUIVALENT PARAMETERS

In the circuit shown in Fig. 1, all the parameters have to be considered as phase components. As a high-order, variable-parameter, multi-variable, nonlinear complex system, it is important to highlight that the magnetizing inductance, the rotor leakage inductance, and the rotor resistance are not constant components and that they have to be determined by several factors, respectively [27], [28], [29]. In addition, it is very difficult to figure out the exact change of all IM parameters simultaneously. Based on reasonable experimental statistics and analyses, it is of great practical significance to investigate the parameter sensitivity to circuit excitation and to simplify the difficulty of parameter acquisition.

1) CORE SATURATION WITH DIFFERENT METHODS

Based on the above analysis, the proposed OSF starting method depends on the motor parameters, and they do have a complex relationship with the saturation of motor core. Generally, the motor saturation point is designed near the point of rated voltage, the increase in driving voltage of induction motor causes the motor saturation to increase.

According to the test data on several IMs made by the authors, the OSF is generally a small value, which results in the starting voltage is inevitably smaller than the one at rated frequency. That is to say, the main magnetic pass is still in a linear state as a whole by using OSF, and the motor saturation is much less than the rated one. Therefore, the effect of the OSF to motor saturation is very small during the starting process with OSF. On the contrary, the starting voltage is the rated one with the direct starting, and the motor saturation phenomenon is much more serious.

2) SENSITIVITY ANALYSES OF IM PARAMETERS

According to the author's previous research on IM parameters [30], [31], which includes IM-1, within the frequency range of 0 - 75 Hz, the parameter sensitivity to input excitation can be summarized as follows:

1) The stator parameters are almost not affected by the changes of driving voltage, current and frequency.
2) L_μ is almost not affected by the driving frequency, but it gradually decreases with the increase of stator current and the saturability of the main magnetic path; R_{Fe} increases with the increase of driving voltage and frequency.
3) Under normal operation, R_2 is almost constant. In locked-rotor state, due to the skin effect on rotor bars, R_2 increases as the frequency rises. The increasing current and frequency may cause the transmission capacity of the rotor leakage magnetic field to be weakened, resulting in the reduction of $L_{2\sigma}$.
4) Generally, R_{Fe} is 40∼80 times larger than R_1, and L_μ is 16∼22 times larger than $L_{1\sigma}$.

The sensitivity of OSF to IM parameters relates with the sensitivities of IM parameters themselves. As can be seen from the above, the main magnetic path of IM is linear in motor starting by using OSF, the core loss of the motor should be very low. In this case, R_{Fe} can be treated as infinite, and has little effect on OSF. In addition, the stator parameters are almost not affected by the changes of driving variables, and can be treated as constants. Therefore, the proposed OSF method is more sensitive to the rotor parameters and magnetizing inductance L_μ.

3) DETERMINATIONS OF STARTING PARAMETERS

At the moment of starting with the OSF starting strategy, the stator and rotor frequency are considered to be the same. Generally, the magnetic saturation point of IM is designed near the rated voltage, which is also verified in our experiments on IM-1. The starting voltage is much lower than the voltage at the magnetic saturation point as the value of OSF is quite small, therefore, although the excitation inductance varies greatly with the current, the starting process is considered to be in linear status rather than saturation status as a whole, the permeability is relatively constant, and the excitation inductance and rotor leakage inductance do not change much. The influence of skin effect on rotor resistance R_2 can also be negligible at the moment of OSF starting, due to the starting frequency is quite low.

During the subsequent starting process, the slip is fluctuant when the switching frequency rises (mentioned in Section IV), the frequency fluctuations and irregular parameter changes on rotor winding make it difficult to determine the rotor resistance and leakage reactance. In order to minimize the influence caused by motor parameter errors, the IM parameters are tested when the main magnetic path is in linear state (LS) and high current state (HS), respectively.

To explore the effect of OSF, the authors utilized the previous test results of Siemens motor IM-1, its nameplate data are shown in Table 1. All the following experiments are carried out under Wye connection, this is for the convenience of obtaining phase voltages and currents, and the theoretical derivation and validation results presented in this paper are not affected by the type of connection of the stator windings. Table 2 shows the parameter values obtained when the main magnetic path of IM-1 is in linear state (LS) and high current state (HS), respectively.

TABLE 1. IM-1 nameplate data.

Parameter	Value
Model	SIMOTICS 0CV3083B
Rated power (W)	750
Rated voltage (V)	220/380
Rated current (A)	3.3/1.9
Rated frequency (Hz)	50/60
Rated speed (r/min)	1440
Pole pairs	2

TABLE 2. Determinations of IM-1 parameters.

Parameter	Symbol	LS	HS
Stator resistance (Ω)	R_1	10.12	10.12
Stator leakage inductance (mH)	$L_{1\sigma}$	34.40	34.40
Iron loss resistance (Ω)	R_{Fe}	4291.60	6393.49
Magnetizing inductance (mH)	L_μ	709.10	543.50
Rotor resistance (Ω)	R_2	6.00	6.89
Rotor leakage inductance (mH)	$L_{2\sigma}$	64.00	33.40

B. DETERMINATION OF STARTING VOLTAGE

As the OSFs are much lower than the rated frequency, and their starting voltages are also much lower than the rated ones. Therefore, an example will be used in the following analysis to determinate the starting voltage. To keep the current within the limit of the IM driver, and to analyze the starting torque obtained with the same starting current, the relationship of starting voltage with current can be expressed as

$$U_1 = \frac{I_1\sqrt{C_{Re}(\omega)^2 + C_{Im}(\omega)^2}}{\sqrt{(R_3R_{\mathrm{Fe}} - \omega^2 L_{2\sigma}L_\mu)^2 + \omega^2(R_{\mathrm{Fe}}L_{2\sigma} + R_3L_\mu + R_{\mathrm{Fe}}L_\mu)^2}} \tag{26}$$

where, both $C_{\mathrm{Re}}(\omega)$ and $C_{\mathrm{Im}}(\omega)$ are frequency response functions

$$C_{\mathrm{Re}}(\omega) = R_2R_1R_{\mathrm{Fe}} - \omega^2\left[R_2L_{1\sigma}L_\mu + s\left(L_{2\sigma}L_\mu R_1 + L_{1\sigma}L_{2\sigma}R_{\mathrm{Fe}} + L_{1\sigma}L_\mu R_{\mathrm{Fe}} + L_{2\sigma}L_\mu R_{\mathrm{Fe}}\right)\right] \quad (27)$$

$$C_{\mathrm{Im}}(\omega) = -s\omega^3 L_{1\sigma}L_{2\sigma}L_\mu + \omega\left[s\left(L_{2\sigma}+L_\mu\right)R_1R_{\mathrm{Fe}} + R_2L_\mu R_1 + R_2\left(L_{1\sigma}+L_\mu\right)R_{\mathrm{Fe}}\right] \quad (28)$$

Ignoring iron loss resistance, (26) can thus be simplified as

$$U_1 = \frac{I_1\sqrt{C_{Re}(\omega)^2 + C_{Im}(\omega)^2}}{\sqrt{R_2^2 + \omega^2 s^2 (L_{2\sigma}+L_\mu)^2}} \quad (29)$$

where

$$C_{\mathrm{Re}}(\omega) = R_2R_1 - \omega^2 S\left(L_{1\sigma}L_{2\sigma} + L_{1\sigma}L_\mu + L_{2\sigma}L_\mu\right) \quad (30)$$

$$C_{\mathrm{Im}}(\omega) = \omega\left[R_2\left(L_{1\sigma}+L_\mu\right) + s\left(L_{2\sigma}+L_\mu\right)R_1\right] \quad (31)$$

IV. STARTING STRATEGY BASED ON OSF

According to (25), the OSF derived by the MST is only related to the slip and parameters of IM, and is much smaller than the rated one, that results in the final speed using OSF may well being far away from the target speed. Therefore, the starting frequency needs to be gradually increased until the motor operates at the target speed during the starting process. According to the Algorithm scheme in Fig. 2, the starting process is realized as follows.

Step 1) Preliminarily, according to the initial value $s(0)$=1, the optimal starting frequency $f(0)$ should be calculated by (25), and then the synchronous speed $n_s(0)$, the target speed $aim\_n(0)$, the speed error $error\_n(0)$, and the starting voltage $U_1(0)$ have to be calculated by (32)-(35), respectively.

Step 2) By combining Step 1) and (22), the following calculations must be made, where $i = 1, 2, 3, \ldots$.

$$s(i) = \frac{aim\_n(i-1) - n_{\mathrm{s}}(i-1)}{aim\_n(i-1)} \quad (32)$$

$$n_{\mathrm{s}}(i) = 60f(i)/p \quad (33)$$

$$aim\_n(i) = k_1 n_{\mathrm{s}}(i) + k_2 \quad (34)$$

$$error\_n(i) = actual\_n - k_1 n_{\mathrm{s}}(i) \quad (35)$$

where, k_1 is defined as the asynchronous coefficient and k_2 as the speed increment coefficient. k_2 determines the iterations and affects the speed of the starting process.

Step 3) Repeat the iterative Step 2) until $n_{\mathrm{s}}(i) \geq set\_n$, then $f(i)$, $n_{\mathrm{s}}(i)$ have to be computed.

$$n_{\mathrm{s}}(i) = set\_n \quad (36)$$

$$f(i) = p \cdot set\_n/60 \quad (37)$$

Step 4) According to the relationship between real-time speed $actual\_n$ and synchronous speed $n_s(i)$, the output frequency f and driving voltage U_1 of the driver can thus be determined.

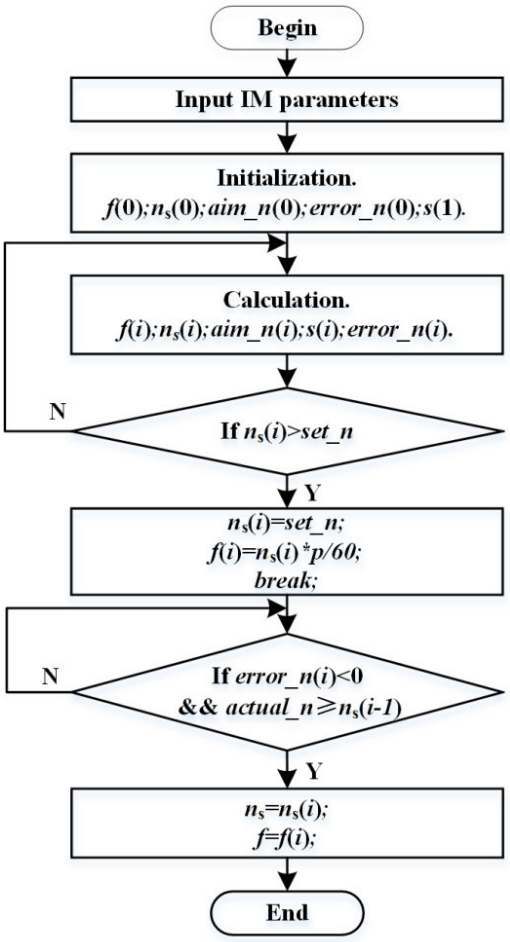

FIGURE 2. Algorithm scheme of variable frequency starting.

V. EXPERIMENTAL VALIDATION

This section aims to prove the validity of the above analyses and investigate the influence of driving state change on OSF. dSPACE MicroLabBox was used to build a rapid control prototype for IM driving system shown in Fig. 3. To facilitate effective comparison and analysis of OSF obtained by OSTPA and MST mentioned in this paper, IM-1 is also used as an experimental object, and the starting torque test and the starting strategy verification are performed, respectively.

A three-phase symmetric system is the basis of this study, in order to minimize the iron losses caused by non-sinusoidal voltage input, the switching frequency of the IGBTs is increased to 20kHz, and only the filtered sinusoidal part of the armature current was used to compute the single-phase equivalent circuit model of three-phase IM.

A. STARTING TORQUE VALIDATION

To investigate the differences of OSF obtained by OSTPA and MST, and the differences between the theoretical values and measured results, other related experiments are utilized and analyzed. The starting torque was measured and calculated on multiple frequency points with the same starting

current, respectively, and two typical current values of 1.4 A and 2.5 A are selected, which represent the LS and HS of the motor, respectively. Figs. 4 and 5 show the comparisons of the theoretical and experimental values for the method mentioned above.

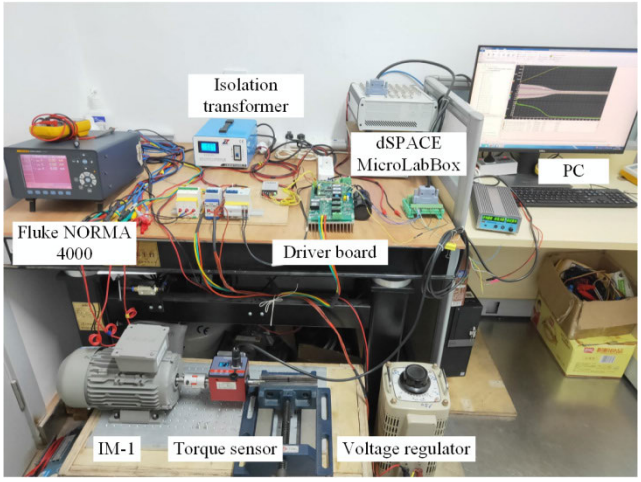

FIGURE 3. Test bench.

As can be seen in Fig. 4, it is clear that the starting torque of IM-1 at a certain driving frequency is much larger than that at the rated frequency. Under a starting current of 1.4 A, the measured OSF of IM-1 occurs at 1.8 Hz, and the corresponding torque is 11.36 times of that at 50 Hz with the same current. The calculated OSFs obtained by OSTPA and MST are 1.42 Hz and 1.49 Hz, respectively. The proposed OSF-MST is almost consistent with the method of OSF-OSTPA, and their change trends are basically consistent with the measured values, and it can be clearly seen that the starting torque of IM at a certain driving frequency is much larger than that at the rated frequency.

The starting torque under 2.5 A starting current is shown in Fig. 5. It can be seen that the trends of the starting torque varying with frequency in the tests are also highly consistent with the theoretical analysis. The torque is 9.43 times of the one at 50 Hz with the same current. The calculated OSFs obtained by OSTPA and MST are 1.48 Hz and 1.59 Hz, respectively. Both the methods of MST and OSTPA prove the existence of OSF, which is same as the one under 1.4 A starting current.

By comparing Figs. 4 - 6 and Table 3, it can be known that:

1) The OSF of IM is discussed by the methods of OSF-MST and OSF-OSTPA from different perspectives, respectively, and clearly confirmed by both the theoretical and experimental results. The starting torque at OSF is much higher than that at rated frequency with the same starting current, which is very effective for improving the starting performance of IM.
2) As can be seen in Fig. 6, the OSF will increases slightly as the starting current increases, that is because the change in driving state causes the motor parameters to change.
3) The slight differences of OSF between the experimental and theoretical results is considered to be the IM parameters are measured in rotating state, which are slightly different from those obtained at stationary state.
4) Compared with the test values, both methods of OSF-MST and OSF-OSTPA have certain errors seen from the figures, the starting torque obtained by MST method proposed in this paper is more in line with the tested one, this phenomenon is exactly caused by the difference between the two analytical methods of OSF.

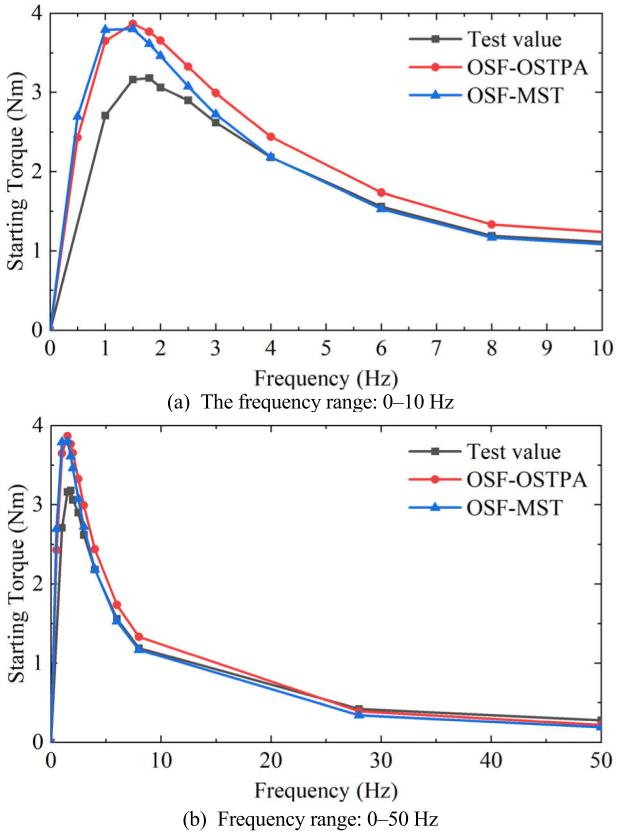

FIGURE 4. IM-1 starting torque with 1.4A starting current.

Although the analytical OSFs obtained by both OSF-MST and OSF-OSTPA methods are highly consistent and can also be matched well with the experimental one, there are some differences in the starting torque between the theoretical calculation and testing results, especially at the points where the torque is larger; see Figs. 4 and 5. The main reasons for this were considered as the errors of the provided IM parameters and the insufficient accuracy of the torque transducer, and should be paid attention to in further research.

B. STARTING STRATEGY VERIFICATION

The existing starting methods for induction motors are mainly direct starting, soft-starting, and discrete frequency starting.

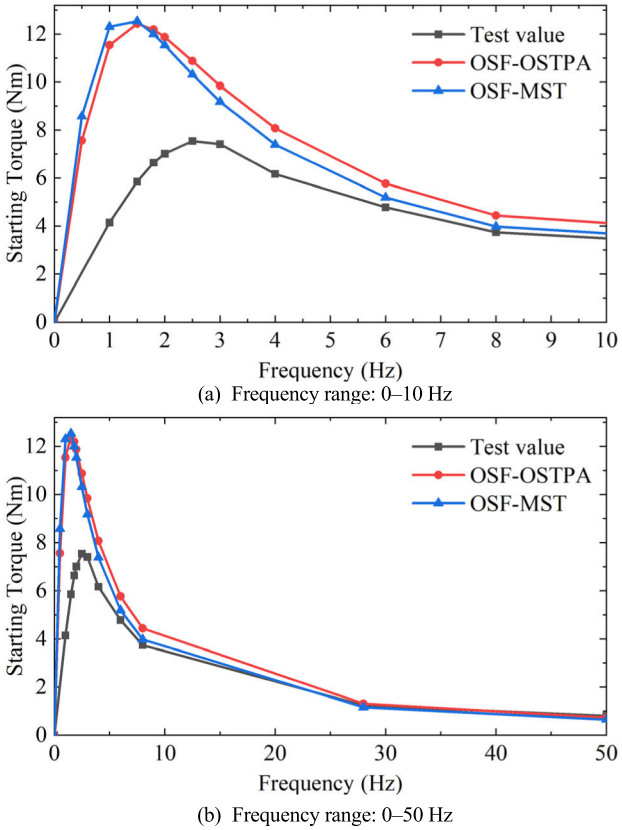

FIGURE 5. IM-1 starting torque with 2.5A starting current.

TABLE 3. Comparison of the experiment results.

Current	Starting Torque (*Nm*)		
	T_C: Conventional starting at 50Hz	T_{OSF}: Starting at OSF	T_{OSF} / T_C
LS (1.4A)	0.28	3.18	11.36
HS (2.5A)	0.8	7.54	9.43

The OSF can be considered as a discrete frequency starting. The starting current and starting torque of induction motor are very high in direct starting method, the soft starter is designed to suppress the starting current with the expense of weakening the starting torque, which makes the duration of starting process may be longer than direct starting, so the direct starting is chose to use for comparison in this study.

It is worth noting that the OSF and its starting strategy discussed here are obtained under a universal model, and do not affect its application conditions. Considering the excessive starting current of induction motor with load and the limitation of experimental conditions, the no-load starting is used for verify the OSF strategy in the following.

The starting processes of IM-1 under different conditions are shown in Figs. 7 - 10. By using the OSF starting strategy mentioned above, the initial starting speed of IM-1 is pulled up quickly and much higher than that of direct starting, which ensures that the motor was activated with maximum starting torque and accelerates the starting process. At the set speed of 1000 r/min and the starting current of 1.4A, the driving

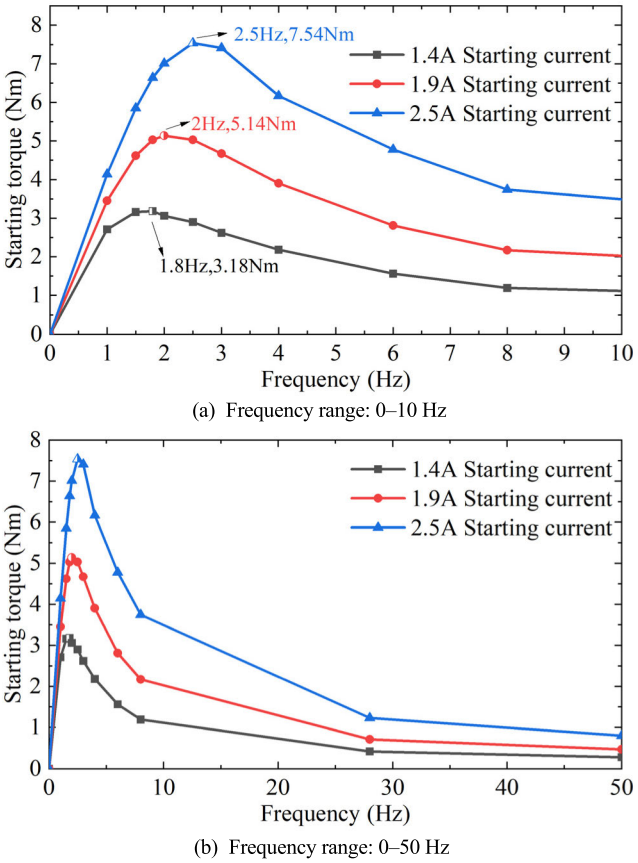

FIGURE 6. Test values of starting torque with different starting current.

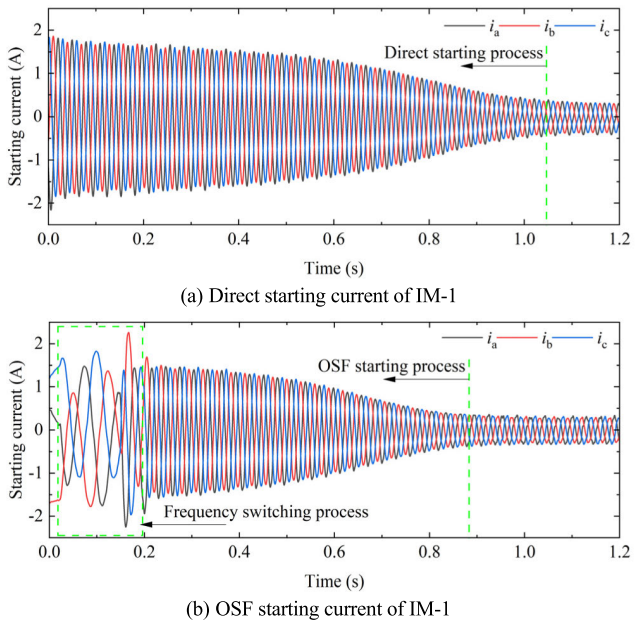

FIGURE 7. IM-1 starting process (I_{st} =1.4A, n = 1000r/min).

voltage at OSF starting is 20V calculated by (26). As can be seen in Figs. 7 and 8, the total starting time of the proposed OSF starting strategy is 0.886s, and has a 13.7% improvement compared to the one at direct starting. Figs. 9 and 10 show

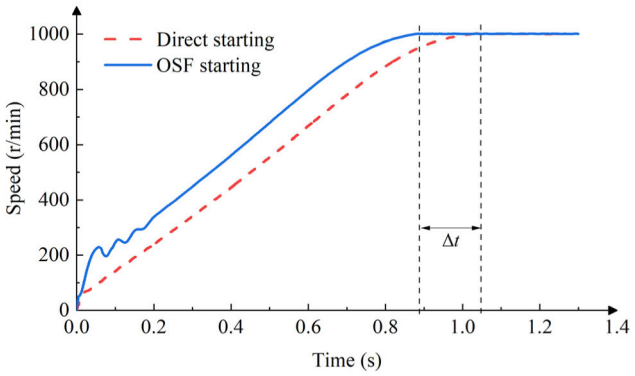

FIGURE 8. Verification of OSF starting strategy (I_{st} = 1.4A, n = 1000r/min).

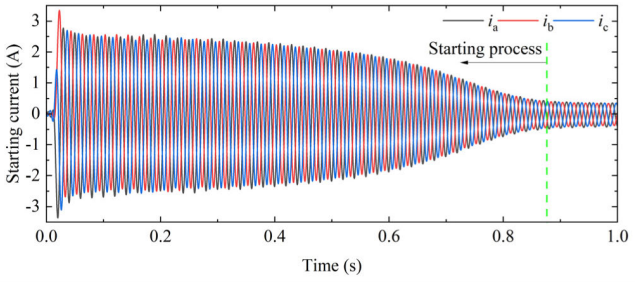

(a) Direct starting current of IM-1

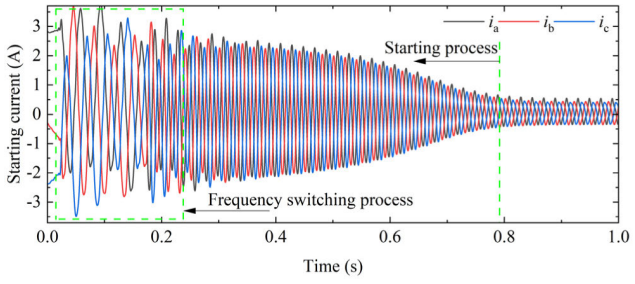

(b) OSF starting current of IM-1

FIGURE 9. IM-1 starting process (I_{st} = 2.5A, n = 1500r/min).

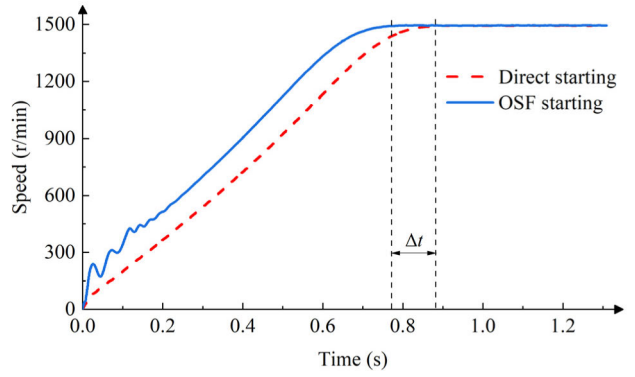

FIGURE 10. Verification of OSF starting strategy (I_{st} = 2.5A, n = 1500r/min).

that, at the set speed of 1500 r/min and starting current of 2.5A, the calculated driving voltage is 35.5V, the OSF starting time is 0.761s, which has a 12.9% improvement compared to the one at direct starting. Therefore, the OSF control strategy possesses better starting performance in terms of both the starting time and starting torque.

However, the speed jitter during IM-1 starting process affects the better performance of OSF starting strategy. The major root for this is caused by frequency switching. Due to the initial OSF is generally small, and the OSF starting strategy has to gradually improve the speed to meet the targeted one by switching the driving frequency. How to achieve a better method for frequency switching is beyond the spirit of this paper, and will be specially focused on in the authors' subsequent work.

VI. CONCLUSION

In this paper, the proposed methodologies for OSF and starting strategy of three-phase IM have been investigated. Based on the electromagnetic torque-frequency characteristic of IM, a complete theoretical analysis of OSF plus the step-by-step starting algorithms have been included to develop a numerical code. In addition, compared with the starting frequency derived from OSTPA, the OSF results of the proposed MST have a good agreement, which proves that the OSF of three-phase IM definitely exists once again. Both the starting torque and starting time of IM are optimized through testing the three-phase squirrel-cage IM with the proposed algorithms. The proposed OSF was derived from the universal T-type equivalent model of IM, taking into account the iron loss. Although the analysis is based on three-phase squirrel-cage IM, the conclusions drawn in this study are theoretically applicable to the other types of IMs. In future research, detailed studies of eliminating speed jitter caused by switching frequency during the starting process will be carried out to thoroughly improve the starting performance of IMs.

REFERENCES

[1] J. Resa, D. Cortes, J. F. Marquez-Rubio, and D. Navarro, "Reduction of induction motor energy consumption via variable velocity and flux references," *Electronics*, vol. 8, no. 7, p. 740, Jun. 2019.
[2] X. Liang and O. Ilochonwu, "Induction motor starting in practical industrial applications," *IEEE Trans. Ind. Appl.*, vol. 47, no. 1, pp. 271–280, Jan. 2011.
[3] M. Digalovski and G. Rafajlovski, "Calculation of starting and breaking times of induction motor electric drives, for different mechanical loads," in *Proc. Int. Conf. Inf. Technol. (InfoTech)*, Sep. 2020, pp. 1–4.
[4] J. Larabee, B. Pellegrino, and B. Flick, "Induction motor starting methods and issues," in *Proc. 52nd Annu. Petroleum Chem. Ind. Conf.*, Oct. 2005, pp. 217–222.
[5] X. Liang, R. Laughy, and J. Liu, "Investigation of induction motors starting and operation with variable frequency drives," in *Proc. Can. Conf. Electr. Comput. Eng.*, vol. 36, 2007, pp. 556–561.
[6] P. Aree, "Starting time calculation of large induction motors using their manufacturer technical data," in *Proc. 19th Int. Conf. Electr. Mach. Syst. (ICEMS)*, Nov. 2016, pp. 1–5.
[7] T. Gundogdu, Z. Zhu, and J. Mipo, "Analysis of coil pitch in induction machines for electric vehicle applications," *IET Electr. Power Appl.*, vol. 14, no. 12, pp. 2525–2536, Oct. 2020.
[8] T. Gundogdu, Z. Zhu, J. Mipo, and S. Personnaz, "Influence of stator and rotor geometric parameters on rotor bar current waveform and performance of IMs," *J. Eng.*, vol. 2019, no. 17, pp. 3649–3654, Jun. 2019.
[9] M. Kong, X. Wang, Z. Li, and P. Nie, "Asynchronous operation characteristics and soft-starting method for the brushless doubly-fed motor," *IET Electr. Power Appl.*, vol. 11, no. 7, pp. 1276–1283, Aug. 2017.

[10] H. J. Lee, S. H. Im, D. Y. Um, and G. S. Park, "A design of rotor bar for improving starting torque by analyzing rotor resistance and reactance in squirrel cage induction motor," *IEEE Trans. Magn.*, vol. 54, no. 3, pp. 1–4, Mar. 2018.
[11] A. Stermecki, I. Ticar, I. Zagradisnik, and P. Kitak, "FEM-based design of an induction motor's part winding to reduce the starting current," *IEEE Trans. Magn.*, vol. 42, no. 4, pp. 1299–1302, Apr. 2006.
[12] A. G. Yetgin, "Investigation of the effects of stator slot permeance on induction motor and obtaining the best starting torque using permeance calculation," *Can. J. Electr. Comput. Eng.*, vol. 43, no. 1, pp. 25–29, Winter 2020.
[13] G. Lee, S. Min, and J.-P. Hong, "Optimal shape design of rotor slot in squirrel-cage induction motor considering torque characteristics," *IEEE Trans. Magn.*, vol. 49, no. 5, pp. 2197–2200, May 2013.
[14] M. A. Badr, A. I. Alolah, and M. A. Abdel-Halim, "A capacitor start three phase induction motor," *IEEE Trans. Energy Convers.*, vol. 10, no. 4, pp. 675–680, Dec. 1995.
[15] H. Wan-Ting, Z. Ya-Jie, R. Si-Ming, and Z. Hai-Yan, "A new starting method for asynchronous induction motor," in *Proc. IEEE 2nd Int. Conf. Comput., Control Ind. Eng.*, vol. 2, Aug. 2011, pp. 341–344.
[16] K. Nagata, T. Okuyama, H. Nemoto, and T. Katayama, "A simple robust voltage control of high power sensorless induction motor drives with high start torque demand," *IEEE Trans. Ind. Appl.*, vol. 44, no. 2, pp. 604–611, Mar. 2008.
[17] K. Nafeesa and S. George, "Optimization of starting performance of thyristorized static switch fed three phase induction motor," in *Proc. Joint Int. Conf. Power Electron., Drives Energy Syst. Power India*, Dec. 2010, pp. 1–5.
[18] A. Nied, J. de Oliveira, R. de F. Campos, R. P. Dias, and L. C. de Souza Marques, "Soft starting of induction motor with torque control," in *Proc. IEEE Ind. Appl. Soc. Annu. Meeting*, vol. 103, Oct. 2008, pp. 1–6.
[19] F. Jiang, C. Tu, Q. Guo, Z. Wu, and Y. Li, "Adaptive soft starter for a three-phase induction-motor driving device using a multifunctional series compensator," *IET Electr. Power Appl.*, vol. 13, no. 7, pp. 977–983, Jul. 2019.
[20] D. F. Wang, Y. N. Wang, J. Yu, L. Cui, and Y. Wang, "Research on hierarchical discrete frequency soft starter of asynchronous motor," *Electr. Power Sci. Eng.*, vol. 34, no. 7, pp. 7–14, Jul. 2018.
[21] A. E. Ginart, R. Esteller, A. Maduro, R. Pinero, and R. Moncada, "High starting torque for AC SCR controller," *IEEE Trans. Energy Convers.*, vol. 14, no. 3, pp. 553–559, Sep. 2002.
[22] K. Q. Zhao, D. Xu, and W. Yi, "New strategy to improve electromagnetic torque at starting in thyristor controlled induction motors," in *Proc. Conf. IEEE Ind. Electron. Soc.*, Apr. 2004, pp. 2555–2561.
[23] F. Zhou, J. L. Cao, J. Liu, and B. Q. Wang, "Optimal switching phase and frequency splitting strategy of discrete frequency conversion soft starting control for asynchronous motor," *Electr. Mach. Control.*, vol. 20, no. 3, pp. 13–19, Apr. 2016.
[24] H. M. Zhang, "High torque soft start technology based on multilevel discrete variable frequency," *Chin. J. Power Source*, vol. 36, no. 9, pp. 1374–1376, Sep. 2012.
[25] K. Q. Zhao, Y. Wang, D. G. Xu, and H. W. Liu, "A new strategy to improve electromagnetic starting torque for thyristor controlled induction motors," *Proc. CSEE*, vol. 24, no. 3, pp. 145–150, Mar. 2004.
[26] H. Chen and C. Bi, "Optimal starting frequency of three-phase induction motor," *IET Electr. Power Appl.*, vol. 16, no. 3, pp. 362–369, Mar. 2022.
[27] A. Boglietti, A. Cavagnino, and M. Lazzari, "Computational algorithms for induction-motor equivalent circuit parameter determination—Part I: Resistances and leakage reactances," *IEEE Trans. Ind. Electron.*, vol. 58, no. 9, pp. 3723–3733, Sep. 2011.
[28] A. Boglietti, A. Cavagnino, and M. Lazzari, "Computational algorithms for induction motor equivalent circuit parameter determination—Part II: Skin effect and magnetizing characteristics," *IEEE Trans. Ind. Electron.*, vol. 58, no. 9, pp. 3734–3740, Sep. 2011.
[29] Z. Ling, L. Zhou, S. Guo, and Y. Zhang, "Equivalent circuit parameters calculation of induction motor by finite element analysis," *IEEE Trans. Magn.*, vol. 50, no. 2, pp. 833–836, Feb. 2014.
[30] H. Chen and C. Bi, "An effective method for determination and characteristic analysis of induction motor parameters," *IET Electr. Power Appl.*, vol. 16, no. 5, pp. 605–615, May 2022.
[31] H. Chen and C. Bi, "Influence of driving state on parameters of three-phase induction motor," in *Proc. IEEE 4th Int. Electr. Energy Conf. (CIEEC)*, May 2021, pp. 1–6.

HAIXU CHEN received the B.S. degree in electrical engineering and automation from North China University of Water Resources and Electric Power, Zhengzhou, China, in 2011, and the M.S. degree in power electronics and power derives and the Ph.D. degree in control science and engineering from the University of Shanghai for Science and Technology, Shanghai, China, in 2014 and 2022, respectively.

He is currently working as a Lecturer of electrical engineering, Huanghuai University, Zhumadian, China. His research interests include analysis and control of high-performance motor drive and electric energy transform.

CHAO BI (Senior Member, IEEE) received the B.S. degree from Hefei University of Technology, in 1982, the M.S. degree from Xi'an Jiaotong University, in 1984, and the Ph.D. degree from the National University of Singapore, in 1994.

He is currently working as the CTO of Fortior Technology (Shenzhen) Company Ltd. His research interests include the analysis, design, test, control and optimization of induction motor, permanent-magnet motor, micro motor, electromagnetic field synthesis, and sustainable energy technology. He has published more than 190 papers in these areas. He got National Technology Award (Singapore) in 2006 for his contributions in precision motor technology.

SEN LI received the B.S. degree in automation from Henan University of Science and Technology, Luoyang, China, in 2012. He is currently pursuing the Ph.D. degree in electrical engineering discipline with the School of Electrical and Information Engineering, Zhengzhou University, Zhengzhou, China.

His research interests include design, analysis, and control of permanent magnet machines.

ZHEN PENG received the B.S. degree from the School of Electrical Engineering and Automation, Xuchang University, Xuchang, China, in 2017, and the Ph.D. degree in control science and engineering from the University of Shanghai for Science and Technology, Shanghai, China, in 2023.

He is currently working as a Lecturer with the School of Automotive and Traffic Engineering, Hubei University of Arts and Science, Xiangyang, China. His research interests include high performance control, driving, and testing of permanent magnet synchronous motors.

ZHONGXIAN CHEN received the B.S. degree in electronic engineering from Zhengzhou University of Light Industry, Zhengzhou, China, in 2007, and the Ph.D. degree in electronic engineering from Southeast University, Nanjing, China, in 2015.

He is currently working as a Lecturer of electronic engineering, Huanghuai University, China. His research interest includes permanent magnet motor design and control.